Improved Global-Local Model to Predict Guided-Wave Scattering Patterns from Discontinuities in Complex Parts

Antonino Spada[a], Margherita Capriotti[b], Ranting Cui[b], Francesco Lanza di Scalea*[b]
[a]Department of Civil, Environmental, Aerospace, and Materials Engineering, University of Palermo, 90128, viale delle Scienze, Ed. 8, Italy; [b]NDE&SHM Laboratory, Department of Structural Engineering, University of California San Diego, La Jolla, CA 92093-0085, USA

ABSTRACT

Ultrasonic guided-wave testing can greatly benefit from (1) an ability to provide quantitative information on the damage that is being detected, and (2) an ability to select the best mode-frequency combination for maximum sensitivity to a given type of damage. Achieving these capabilities in complex structures (e.g. nonprismatic structures such as a stiffened panel in aerospace fuselages) is a nontrivial task. This paper will discuss an improved Global-Local (GL) method where the geometrical "local" discontinuity (e.g. the stiffener) is modelled by traditional FE discretization and the rest of the structure ("global" part) is modelled by Semi-Analytical Finite Element (SAFE) cross-sectional discretization. The boundaries of the "local" domain and the "global" domain are then matched in terms of wave displacement and stresses. GL models have been proposed in the past using theoretical (Lamb) wave solutions that only apply to isotropic plates. The authors have also previously studied GL methods using the SAFE approach for application to multi-layered anisotropic plates for which theoretical solutions are either not existent or hard to obtain. This work will extend recent research on these methods by optimizing the Matlab routine that is used to run the GL code, correcting some formulation errors that were present in the previous edition, and studying the specific case of a composite panel stiffened with co-cured stringers that is representative of modern commercial aircraft construction (e.g. Boeing 787). The newly-formulated GL method will be shown to provide excellent results that can help designing a guided-wave test on these aircraft components for optimum detection of relevant damage that can be induced by impacts (including skin delaminations, stringer heel cracks, and stringer to skin disbonds). Other applications of the GL methods beyond stiffened aircraft panels will be discussed.

Keywords: guided waves, scattering, global-local method, semi-analytical finite element method

1. INTRODUCTION

Ultrasonic testing has been extensively used in the last decades as one of the most promising nondestructive methods to assess the integrity of many kind of structures. In particular, "guided" elastic waves are nowadays increasingly used to probe structural components with a waveguide geometry such as plates, rods, pipes. They have the capability to reach long propagation distances maintaining a sufficient sensitivity to small structural anomalies owing to the relatively large frequencies. A guided wave is obtained as the combination of several wave modes propagating simultaneously. Given this multimode character, together with its dispersive characteristic, closed form solutions are available for simple geometries without defects. When the propagation of the guided wave involves structures with discontinuities such as defects or abrupt changes of the geometry (e.g. insertion of a stiffener), purely theoretical predictions are either non-existent or hard to obtain.

Transportation systems via air or land use vehicles subjected to increasingly higher velocities and external loads. To prevent as much as possible structural failures, which can lead to catastrophic consequences from both the human and the economic points of view, innovative materials are employed. Innovation is in reducing weight maintaining the characteristics of strength and stiffness of the structure. Fiber-reinforced composite materials perform this task, but the complexity of the manufacturing process, together with the severity of external service loads, can develop several defects that need to be detected and quantified through nondestructive techniques.

* *flanza@ucsd.edu*; phone *+1 858-822-1458*

Analytical solutions of guided waves propagation through multi-layered structures can be found in Rose[1] using the global matrix or transfer matrix methods. An improved analytical approach to predict Lamb waves scattering from a geometrical discontinuity (such as a thickness change in isotropic plates or the presence of a horizontal crack) is followed by Poddar and Giurgiutiu[2-3] and Haider et al.[4]

A second way to face with these problems is using numerical tools. Since the numerical results are sensitive to the case of small wavelength propagation, it is not optimum to run a finite element (FE) analysis extended to the entire structure, because the great number of elements needed to reach an accurate result makes the analysis not computationally efficient. However, considering that the discontinuity is localized in a small region with respect to the total dimensions of the structural element, a hybrid Global-Local approach is the best solution. Hybrid methods couple the solution available analytically in the "global" regular region with that applicable numerically in the "local" defected region. A hybrid approach based on a FE discretization of the local region was applied by Goetschel et al.[5], Karunasena et al.[6], Rattanawangcharoen et al.[7], Mal and Chang[8], Zhou and Ichchou[9]. Applications were dedicated to axial-symmetric scattering problems, axial-symmetric inclusions in homogeneous isotropic media, isotropic plates with notches and rivet-hole cracks, reflections from free edges, etc. A hybrid approach employing the boundary element method (BEM) for the local region is instead at the base of the applications of Galan and Abascal[10-11] on semi-infinite plates, plates with inclusions, different cracks and materials.

In the referenced works analytical solutions are considered for the global region, but this part is generally constituted by a plate with a single isotropic material. The easiness to obtain theoretical guided wave solutions in presence of anisotropic composite laminate with a general number of layers is strongly reduced. For this reason, in other works the behavior in the global region is simulated exploiting the advantages of a Semi-Analytical Finite Element method (SAFE). Hayashi et al.[12], Bartoli et al.[13], Marzani et al.[14] discretized in finite elements the cross-section of the laminated composite waveguide, maintaining the known analytical harmonic solution of the displacement component in the propagation direction of the guided wave. Srivastava and Lanza di Scalea[15] applied the SAFE in the GL scattering problem of composite plates of arbitrary number of layers with delamination defects.

This paper will discuss an improved GL method where the geometrical local discontinuity is modelled by traditional FE discretization and the global part is modelled by SAFE cross-sectional discretization. The boundaries of the local and the global domains are then matched in terms of wave displacement and stresses. This work will extend recent research on the GL method (Srivastava and Lanza di Scalea[15]) by optimizing the Matlab routine used to run the GL code, correcting some formulation errors that were present in the previous edition, and studying the specific case of a composite panel stiffened with co-cured stringers that is representative of modern commercial aircraft construction (e.g. Boeing 787). The newly-formulated GL method will be shown to provide excellent results that can help designing a guided-wave test on these aircraft components for optimum detection of relevant damage that can be induced by impacts (including skin delaminations, stringer heel cracks, and stringer to skin disbonds). A second application on a 136lb AREMA cross-section rail with a defected head is also shown, in order to prove the versality and potentiality of the method to face with problems of different nature and complexity.

2. THEORETICAL FORMULATION

Let us consider the general scattering case of Fig. 1. An incident time harmonic guided wave travelling along the x positive direction in a prismatic region (global region) is scattered into reflected and transmitted waves after interacting with a local region with geometrical discontinuities (e.g. build-ups) and/or structural defects (e.g. cracks, delaminations, etc.).

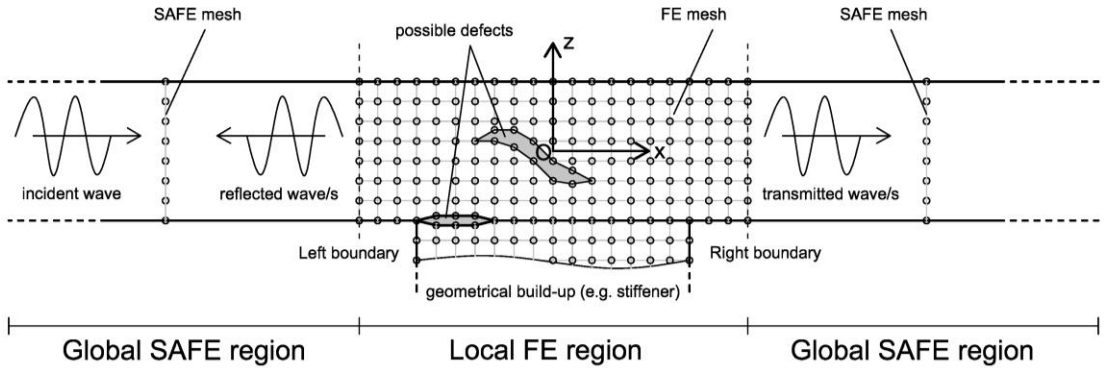

Figure 1. Geometrical representation of the scattering of an incident wave in reflected and transmitted waves from a local region including possible defects and/or geometrical build-ups, with indication of the adopted discretization strategies in each region.

The SAFE method is adopted to discretize the global region, while a classical FE mesh is employed for the local part.

The approximate displacement $\mathbf{u}_h^{\mathrm{g}-e}$ within a single element of the global region can be written as:

$$\mathbf{u}_h^{\mathrm{g}-e}\left(x,y,z,t\right)=\mathbf{N}^{\mathrm{g}}\left(y,z\right)\mathbf{d}^{\mathrm{g}-e}\,e^{i\left(\xi x-\omega t\right)}, \tag{1}$$

where $\mathbf{d}^{\mathrm{g}-e}$ and $\mathbf{N}^{\mathrm{g}}$ are the vector of nodal displacements and the shape function matrix of the global element, respectively. x is the propagation direction, ξ the wavenumber and ω the circular frequency of the propagating wave.

Similarly, the displacement $\mathbf{u}_h^{\ell-e}$ of a point inside an element of the local part is:

$$\mathbf{u}_h^{\ell-e}\left(x,y,z,t\right)=\mathbf{N}^{\ell}\left(x,y,z\right)\mathbf{d}^{\ell-e}\,e^{-i\omega t}, \tag{2}$$

where $\mathbf{d}^{\ell-e}$ is the vector of nodal displacements and $\mathbf{N}^{\ell}$ the shape function matrix of the local element.

With a look to Fig. 1, it is therefore possible to assume that the displacements at nodes on the left boundary are a combination of displacements given by the incident wave and the reflected waves:

$$\mathbf{q}_{lB}=\mathbf{q}_{incident}+\mathbf{q}_{reflected}, \tag{3}$$

while the displacements at nodes on the right boundary are obtained only if transmitted waves are present:

$$\mathbf{q}_{rB}=\mathbf{q}_{transmitted}. \tag{4}$$

If the symbol $\mathbf{\Phi}$ is used to represent the generic mode shape, and the factor $e^{-i\omega t}$ is omitted for simplicity, Eqs. (3) and (4) are explicitly rewritten as:

$$\mathbf{q}_{lB}=\mathbf{\Phi}_{in}^{+}\,e^{i\left[\xi_{in}^{+}\left(d_s-x_{lB}\right)\right]}+\sum_{j=1}^{N_M}A_j^{-}\,\mathbf{\Phi}^{(j)^{-}}e^{i\left(-\xi_j^{-}x_{lB}\right)}, \tag{5}$$

$$\mathbf{q}_{rB}=\sum_{j=1}^{N_M}A_j^{+}\,\mathbf{\Phi}^{(j)^{+}}e^{i\left(\xi_j^{+}x_{rB}\right)}, \tag{6}$$

where the superscript "+" represents a wave travelling in the right direction and the superscript "-" a wave travelling in the left direction. The subscript "in" refers to an incident wave, the subscript "j" to the generic reflected or transmitted mode among the N_M ones included in the analysis. d_s, x_{lB} and x_{rB} measure the distances of the source, left boundary and right boundary respectively from the origin of the reference system, which we fixed in correspondence of the middle point of the local region. Finally, A_j is the complex amplitude of the generic mode. The incoming mode is imposed.

Mode shapes and correspondent wavenumbers and circular frequencies are derived by solving a generalized eigenproblem.

By imposing the principle of virtual displacement on the local region, and separating the contribute of the inner (I) and boundary (B) degrees of freedom, the following equilibrium equations hold:

$$\begin{bmatrix} \mathbf{S}_{II} & \mathbf{S}_{IB} \\ \mathbf{S}_{BI} & \mathbf{S}_{BB} \end{bmatrix} \begin{bmatrix} \mathbf{U}_I^{\ell} \\ \mathbf{U}_B^{\ell} \end{bmatrix} = \begin{bmatrix} \mathbf{0} \\ \mathbf{F}_B^{\ell} \end{bmatrix}, \tag{7}$$

where

$$\mathbf{S} = \mathbf{K}^{\ell} - \omega^2 \mathbf{M}^{\ell} \tag{8}$$

is the dynamic stiffness matrix of the local region, being $\mathbf{K}^{\ell}$ and $\mathbf{M}^{\ell}$ the stiffness and mass matrices. The vector of displacements is also partitioned in displacements of inner nodes ($\mathbf{U}_I^{\ell}$) and displacements of boundary nodes ($\mathbf{U}_B^{\ell}$). The force vector is instead non-null only at the two boundaries of the local region, since the internal stresses transmitted between the global and the local regions act as external tractions at left and right boundaries for the local part. The displacement and force vectors at boundary can be explicitly written as:

$$\mathbf{U}_B^{\ell} = \begin{bmatrix} \mathbf{q}_{lB}^T & \mathbf{q}_{rB}^T \end{bmatrix}^T \tag{9}$$

$$\mathbf{F}_B^{\ell} = \begin{bmatrix} \mathbf{f}_{lB}^T & \mathbf{f}_{rB}^T \end{bmatrix}^T \tag{10}$$

where

$$\mathbf{f}_{lB} = -\mathbf{F}_{in}^{+} e^{i\left[\xi_{in}^{+}\left(d_s - x_{lB}\right)\right]} - \sum_{j=1}^{N_M} A_j^{-} \mathbf{F}^{(j)^{-}} e^{i\left(-\xi_j^{-} x_{lB}\right)}, \tag{11}$$

$$\mathbf{f}_{rB} = -\sum_{j=1}^{N_M} A_j^{+} \mathbf{F}^{(j)^{+}} e^{i\left(\xi_j^{+} x_{rB}\right)}, \tag{12}$$

with $\mathbf{F}_{in}^{+}$, $\mathbf{F}^{(j)^{-}}$ and $\mathbf{F}^{(j)^{+}}$ the consistent nodal force vectors for the incident, j-th reflected wave and j-th transmitted wave, respectively.

Equilibrium equation (7) can be statically condensed. The unknowns A_j^{-} and A_j^{+} are determined through the least square method.

If Γ is the area of the cross-section normal to the propagation direction ***n***, the energy flux carried by the j-th reflected or transmitted wave along the ***n*** direction can be evaluated as

$$E^{(j)} = \int_{\Gamma} \mathbf{P}^{(j)} \bullet \mathbf{n} \, d\Gamma, \tag{13}$$

where $\mathbf{P}^{(j)}$ indicates the Pointing vector of the j-th mode. The conservation of energy is therefore ensured if the following expression is valid:

$$E_{in} = \sum_{j=1}^{N_M} \left(E_{\text{Refl}}^{(j)} + E_{Transm}^{(j)} \right). \tag{14}$$

3. APPLICATION 1: SCATTERING FROM SKIN-TO-STRINGER ASSEMBLY OF COMPOSITE AIRCRAFT PANELS

The geometry of the analyzed panel is shown in Fig. 2. It represents a scaled version of a skin-to-stringer assembly found commercially for aircrafts. This assembly is of interest because it constitutes a suitable application of ultrasonic guided-wave inspections for structural damage (Capriotti et. al.[16]). In this section two results will be shown. First, a comparison between the cases skin-to-stringer vs skin only will demonstrate the effect of the geometrical discontinuity in pristine

conditions. Second, the results of the comparison between the scattering effects in the skin-to-stringer assembly obtained when the damage shown in Fig. 2 is present with respect to the pristine conditions will be discussed.

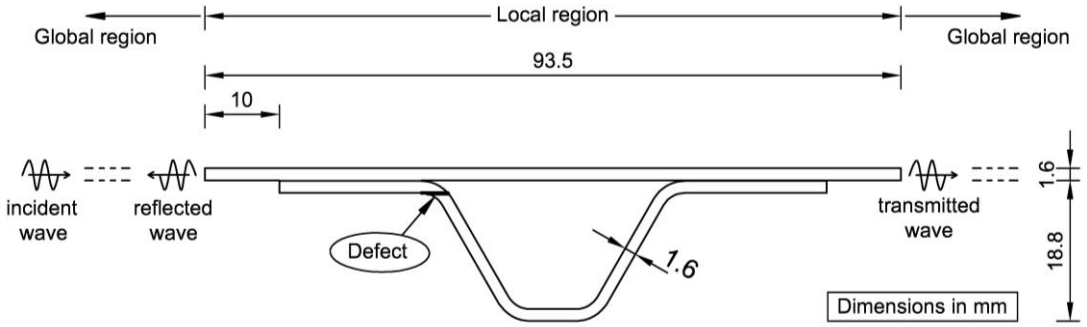

Figure 2. GL model of the composite skin-to-stringer assembly, with indication of the defect considered in this study.

Skin and stringer are both 8-layers of $[0/+45/-45/0]_S$ carbon-epoxy unidirectional laminae with a total thickness of 1.6 mm. At the interface between skin and stringer there is an additional 0° lamina. The density of each lamina is 1530 kg/cm^3 and the elastic properties in the principal direction of material symmetry are given in Table 1, where 1 is the fiber direction while 2 and 3 lay in the plane orthogonal to direction 1. The local region was discretized using a total of 12376 quadrilateral isoparametric linear elements, the global region with 16 monodimensional isoparametric linear elements. The size of the elements was chosen in order to respect the wavelength/element size minimum ratio. The correspondent dispersion curves in the 1-500 kHz frequency range are reported in Fig. 3. As it can be seen, four modes are detected in this frequency range, with the first three fundamental modes and one higher mode (m_4).

In Fig. 4 the comparison between the reflection and transmission spectra for the skin-only case and the skin-to-stringer assembly case is reported. The result clearly shows how the presence of the geometrical discontinuity strongly affects the response. In the skin-only case in pristine conditions no scattering takes place, as the structure behaves as a plate and the incoming mode is totally transmitted without any conversion (Fig. 4a-b).

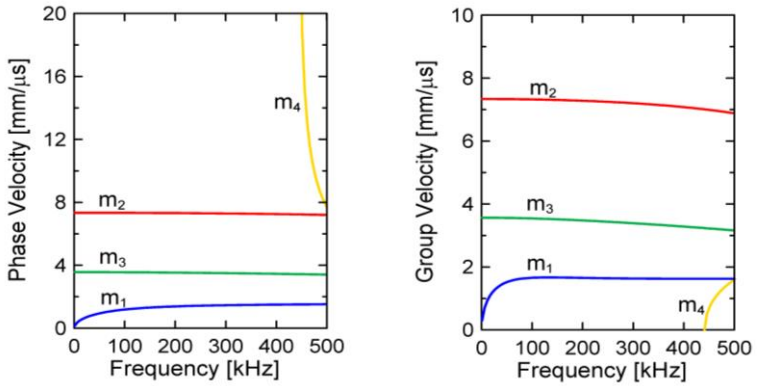

Figure 3. (a) Phase velocity dispersion curves and (b) group velocity dispersion curves for the $[0/+45/-45/0]_S$ composite.

Table 1. Elastic properties for the CFRP lamina.

Property	GPa	Property	GPa
C_{11}	135.00	C_{23}	8.51
$C_{12} = C_{13}$	5.70	C_{44}	2.87
$C_{22} = C_{33}$	14.20	$C_{55} = C_{66}$	4.55

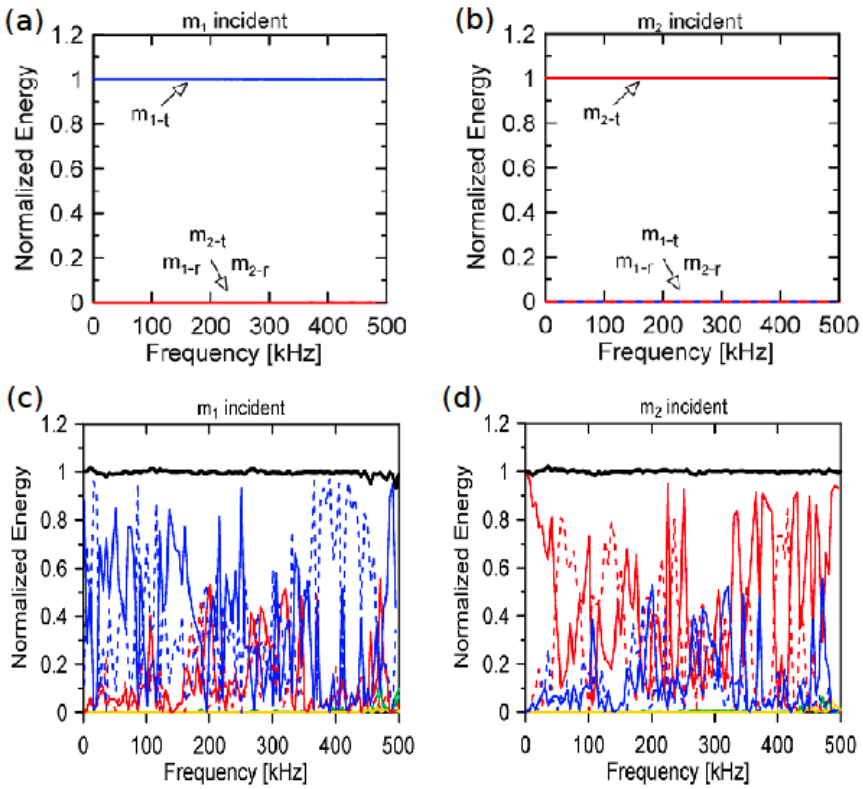

Figure 4. Transmission and reflection spectra for the skin-only case in pristine conditions having a m_1 incoming mode (a) or a m_2 incoming mode (b). Transmission and reflection spectra for the skin-to-stringer case in pristine conditions having a m_1 incoming mode (c) or a m_2 incoming mode (d).

In the skin-to-stringer case, even ifstill in pristine conditions, many conversions take place. For an incident m_1 mode (Fig. 4c), most of the energy is transmitted and reflected as the same m_1, with little mode conversion into m_2 except some specific frequencies where the m_2 mode is transmitted more then m_1. Besides, the m_1 mode is more transmitted below 250 kHz (up to 80% of transmission) with respect to higher frequencies (up to 60% of transmission), with almost complete reflections in the 350-450 kHz range. For an incident m_2 mode (Fig. 4d), strong conversions appear in the range 150-350 kHz, but as before most of the energy is transmitted and reflected as m_2, with higher levels of transmission in the higher 300-500 kHz range and higher levels of reflections around specific frequencies.

In all four cases the computed total energy spectrum is one or close to one, which satisfies the conservation of energy.

In Fig. 5 the effect of damage in the skin-to-stringer assembly with respect to the pristine case is shown. The considered damage is the heel crack of Fig. 2. The results are presented in terms of "difference spectra" for the transmission modes only, in order to highlight the changes in energy absorption (negative values in the difference spectra) or in wave transmission (positive values in the difference spectra).

Analyzing the transmitted m_1 energy for an incoming m_1 (Fig. 5a), a very good sensitivity in the lower frequencies zone is visible: the flexural nature of the mode interacts with the crack and is absorbed by it, reaching a peak of absorption of 90% at 250 kHz and of 70% at 75 and 160 kHz. An increasing in transmission of around 50% is instead recovered at 115 and 195 kHz. The transmitted m_2 for an incoming m_2 (Fig. 5d) also shows a very good detectability of the defect, if used in the higher frequency regime (above 350 kHz), where less than the 20% of the energy can travel to the right boundary. No differences with respect to the pristine case are shown below 200 kHz. From Figs. 5b-c it is clear how the presence of the defect reduces almost totally mode conversions from m_2 to m_1 mode (Fig. 5b) and from m_1 to m_2 mode (Fig. 5c). In these two cases energy absorption is of the order of 40% in the range 200-350 kHz.

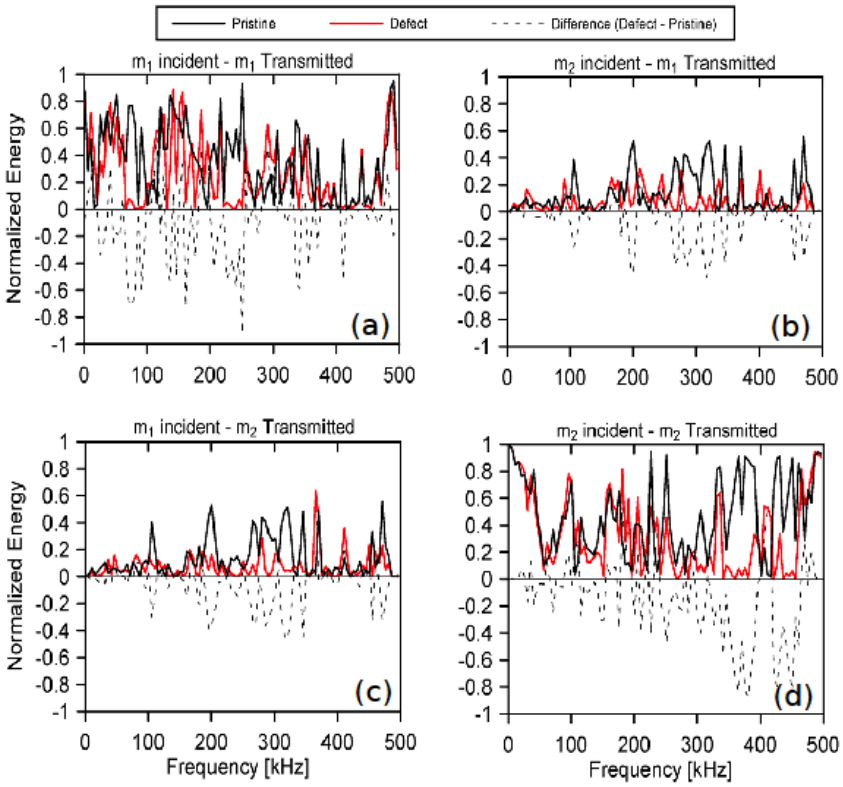

Figure 5. Wave transmission spectra for pristine, defect and (defect-pristine) difference for: (a) m_1 transmitted wave with respect to m_1 incident wave; (b) m_1 transmitted wave with respect to m_2 incident wave; (c) m_2 transmitted wave with respect to m_1 incident wave; (d) m_2 transmitted wave with respect to m_2 incident wave.

4. APPLICATION 2: SCATTERING FROM DAMAGE IN THE HEAD OF A 136LB AREMA SECTION RAIL

The geometry of the analyzed case is shown in Fig. 6.

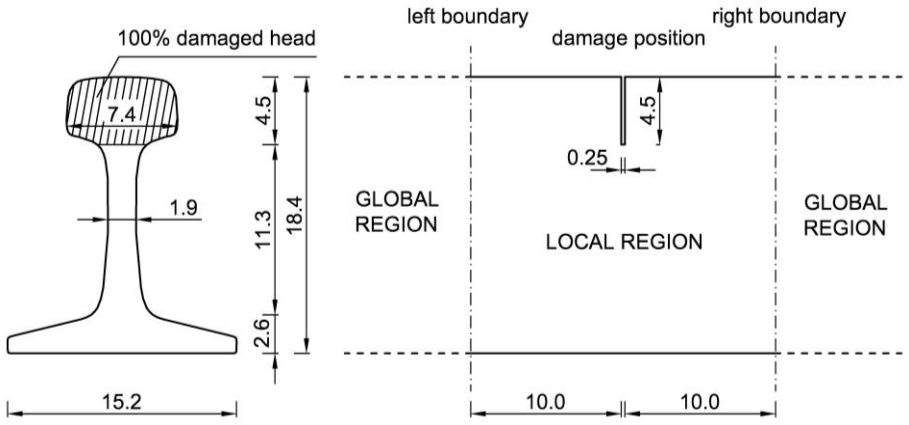

Figure 6. 136lb AREMA section rail with indication of the dimensions of the analyzed local region and location of the 100% damaged head. Dimensions are in cm. Cross-sectional front view (left), lateral view (right).

The total length of the local part considered for the analysis is 20 cm. This length was the maximum one allowed by the power of the computer used for the analysis, on the base of the considered discretization. According to the propagation velocity of the transverse waves obtained from the dispersion curves depicted in Fig. 7, the local region has been discretized in 22884 wedge linear elements, arranged on 81 columns. The head area is around 30 cm^2, with a height of 4.5 cm. Damage is reproduced by eliminating the elements of the head in the 41st column.

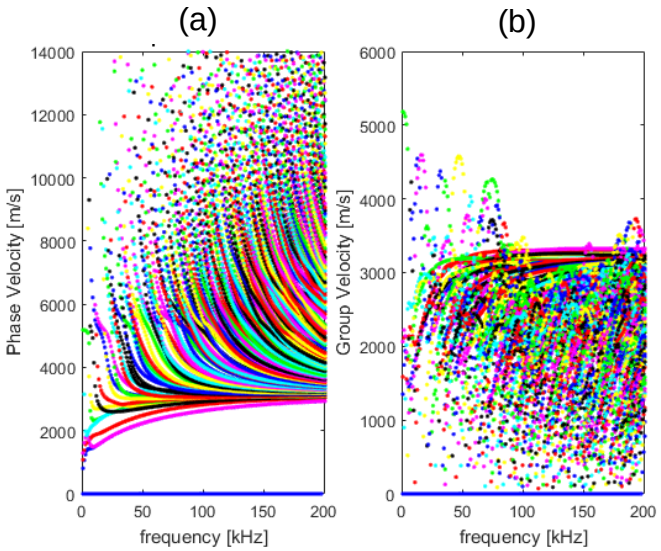

Figure 7. Dispersion curves for the 136lb AREMA section rail, according to the chosen cross-section FE discretization. (a) phase velocity; (b) group velocity.

From Fig. 7, where the 0-200 kHz range is covered, it is possible to note the high number of modes found at each frequency. It is therefore necessary to understand which modes can be the most suitable for damage detection in the head of the rail. For the sake of simplicity, the fourth mode is chosen in this application as the incoming mode for the GL approach. The fourth mode is a compressive mode in the propagation x-direction and is shown in Figs. 8a-b at the two frequencies 1 kHz (Fig. 8a) and 11 kHz (Fig. 8b).

The transmission and reflection spectra for the cases of pristine and damaged rail are instead reported in Fig. 9 for the range 11-180 kHz.

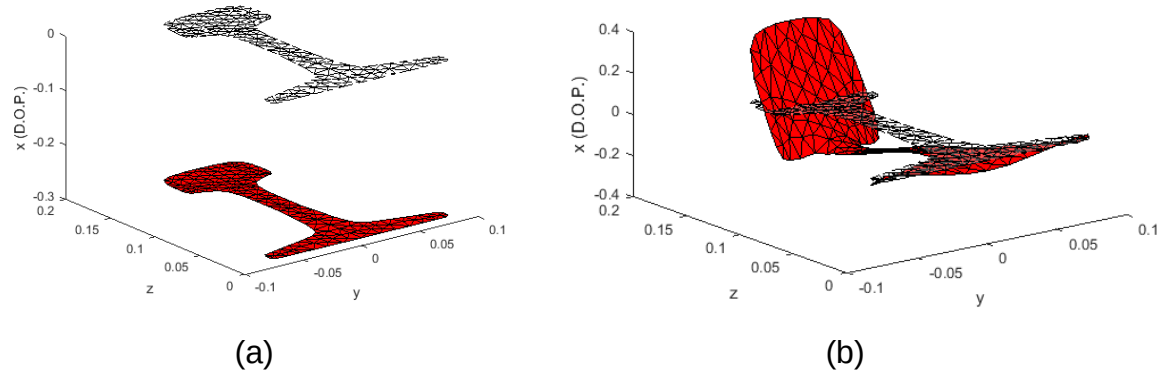

Figure 8. Mode shape of the fourth mode at (a) 1 kHz and (b) 11 kHz.

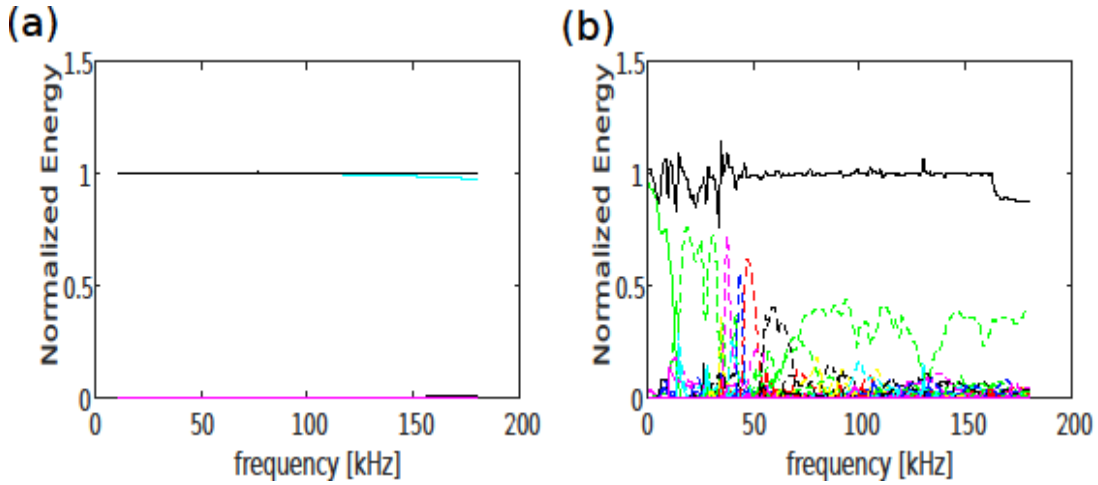

Figure 9. Transmission and reflection spectra for the (a) pristine rail and (b) damaged rail in the case of the incoming fourth mode.

In the case of a pristine rail (Fig. 9a) the incoming wave is totally transmitted, and the conservation of energy is fully respected. At higher frequencies (>130 kHz) also the effect of higher modes is visible, since the incoming mode starts to convert into other transmitted mode shapes. In the case of a damaged rail (100% of damage in the head, Fig. 9b), the energy conservation is respected in the range 40-160 kHz. Below 40 kHz an error of maximum 20 % is obtained, due to the neglected contribution of the evanescent modes to the total energy into the analysis. This means that the two boundaries are not sufficiently far from the damage location to avoid the presence of evanescent modes. At higher frequencies (more than 160 kHz), a second fall of total energy is visible. This second reduction is due to the considered number of scattered modes. It is possible to notice how the presence of the damage causes many conversions into other modes. Strong reflections of the same mode and other converted modes are also recovered. The incoming wave is reflected with the same mode shape below 40 kHz and from 70 kHz till the end. Between 40 and 70 kHz other four modes are reflected with an energy greater than 40%, while generally all other modes are transmitted or reflected carrying an energy below the 20%.

5. CONCLUSIONS

This work proposes a GL method to predict and study ultrasonic guided wave propagation into complex structures, with and without discontinuities. The implementation of such techniques guides the mode-frequency selection for NDE inspections of the skin-to-stringer assembly in aerospace structures and head defects in railroad tracks. For example, the first flexural mode (m_1) can be used to inspect the stiffened skin using frequencies up to 200 kHz, in a trough transmission modality, while frequencies below 40 kHz or above 70 kHz for mode m_4 should be used to assess the head of a rail, preferably in a pulse-echo mode. The obtained transmission/absorption ("difference spectra") are extremely useful to interpret the outcome of experimental tests, where multiple modes of increased/reduced amplitude with respect to the pristine case are present and difficult to evaluate. For example, when inspecting the composite panel at 115 kHz, a recovery of the same m_1 mode should not be mistaken for a sound condition of the skin-to-stringer, but acknowledged as a heel crack. Respectively, an almost halved m_4 mode in reflection should be interpreted as a 100% defected head of the inspected rail track.

These results can be extended to a variety of damage cases and structures. Current work is also focused on the computation of a time domain forced solution of such cases, to be compared to experimental tests.

ACKNOWLEDGMENTS

Part of this work was funded by the Federal Aviation Administration Joint Center of Excellence for Advanced Materials (FAA Cooperative Agreement 12-c-AM-UCSD). A. Spada acknowledges the financial support of the Fulbright Program for the fulfillment of the project E0584038 “Analytical-Numerical models for the simulation of ultrasonic guided wave propagation in composite structures”.

REFERENCES

[1] Rose, J. L., [Ultrasonic guided waves in solid media], Cambridge University Press (2014).
[2] Poddar, B., and Giurgiutiu, V., "Scattering of Lamb waves from a discontinuity: An improved analytical approach", Wave Motion 65, 79-91 (2016).
[3] Poddar, B., and Giurgiutiu, V., "Complex modes expansion with vector projection using power flow to simulate Lamb waves scattering from horizontal cracks and disbonds", The Journal of the Acoustical Society of America 140(3), 2123-2133 (2016).
[4] Haider, M. F., Bhuiyan, M. Y., Poddar, B., Lin, B., and Giurgiutiu, V., "Analytical and experimental investigation of the interaction of Lamb waves in a stiffened aluminum plate with a horizontal crack at the root of the stiffener", Journal of Sound and Vibration 431, 212-225 (2018).
[5] Goetschel, D. B., Dong, S. B., and Muki, R., “A global local finite element analysis of axisymmetric scattering of elastic waves”, Journal of Applied Mechanics 49(4), 816-820 (1982).
[6] Karunasena, W. M., Liew, K. M., and Kitipornchai, S., “Hybrid analysis of Lamb wave reflection by a crack at the fixed edge of a composite plate”, Computer methods in applied mechanics and engineering 125(1-4), 221-233 (1995).
[7] Rattanawangcharoen, N., Zhuang, W., Shah, A. H., and Datta, S. K., “Axisymmetric guided waves in jointed laminated cylinders”, Journal of Engineering Mechanics 123(10), 1020-1026 (1997).
[8] Mal, A., and Chang, Z., “A semi-numerical method for elastic wave scattering calculations”, Geophysical Journal International 143(2), 328-334 (2000).
[9] Zhou, W. J., and Ichchou, M. N., “Wave scattering by local defect in structural waveguide through wave finite element method”, Structural Health Monitoring 10(4), 335-349 (2011).
[10] Galán, J. M., and Abascal, R., “Numerical simulation of Lamb wave scattering in semi-infinite plates”, International Journal for Numerical Methods in Engineering 53(5), 1145-1173 (2002).
[11] Galán, J. M., and Abascal, R., “Boundary element solution for the bidimensional scattering of guided waves in laminated plates”, Computers & structures 83(10-11), 740-757 (2005).
[12] Hayashi, T., Song, W. J., and Rose, J. L., “Guided wave dispersion curves for a bar with an arbitrary cross-section, a rod and rail example” Ultrasonics 41(3), 175-183 (2003).
[13] Bartoli, I., Marzani, A., Lanza di Scalea, F., and Viola, E., “Modeling wave propagation in damped waveguides of arbitrary cross-section”, Journal of Sound and Vibration 295(3-5), 685-707(2006).
[14] Marzani, A., Viola, E., Bartoli, I., Lanza di Scalea, F., and Rizzo, P., “A Semi-analytical Finite Element Formulation for Modeling Stress Wave Propagation in Axisymmetric Damped Waveguides”, Journal of Sound and Vibration 318(3), 488-505 (2008).
[15] Srivastava, A., and Lanza di Scalea, F., “Quantitative structural health monitoring by ultrasonic guided waves”, Journal of Engineering mechanics 136(8), 937-944 (2010).
[16] Capriotti, M., Kim, H. E., Lanza di Scalea, F., and Kim, H., “Non-Destructive inspection of impact damage in composite aircraft panels by ultrasonic guided waves and statistical processing”, Materials 10(6), 616 (2017).